JOURNAL OF CATALYSIS 134, 713–730 (1992)

The Study of Ethane Dehydrogenation in a Catalytic Membrane Reactor

ALTHEA M. CHAMPAGNIE, THEODORE T. TSOTSIS,[1] RONALD G. MINET, AND ERIC WAGNER*

*Department of Chemical Engineering, University of Southern California, Los Angeles, California 90089-1211; and *Kinetic Technology International, Inc., 1333 South Mayflower Avenue, Monrovia, California 91016*

Received June 14, 1991; revised November 6, 1991

Membrane reactors have the capability of combining reaction and separation in a single unit operation. The membrane selectively removes one or more product species. For a number of reactions, whose yields are limited by thermodynamic equilibrium, this results in an increase in the reactor conversion and a corresponding increase in product yield. One such reaction is the catalytic dehydrogenation of ethane. This reaction was studied in an isothermal high-temperature shell-and-tube membrane reactor, containing an alumina ceramic membrane tube impregnated with platinum. A theoretical model was developed for this reactor, based on isothermal conditions and plug-flow behavior. The model shows reasonable agreement with the experimental data.

INTRODUCTION

Many industrial catalytic reactions have relatively low yields due to thermodynamic equilibrium limitations. Ethane dehydrogenation to ethylene is a typical example. Thermodynamic equilibrium conversions of less than 30 mol% are obtained at 700°C. For a number of other reactions, the yield is limited by low selectivity due to undesirable side reactions or slow kinetics, which may be due to reaction product inhibition. Methane oxidation to methanol is such an example. The high temperatures and pressures needed to produce acceptable yields for these reactions often create technical complications and require expensive process equipment and/or specialized catalysts. High-temperature catalytic membrane reactors, which combine simultaneous reaction and separation in a single unit operation, may, for a number of such reactions, solve the yield problems discussed above.

Membrane reactors have in the past found use in the field of biotechnology. Applications include the reduction of cheese whey to peptides (*1*), the reaction of starch to maltose (*1*), and pectin degradation (*2*). The reactors used for these low-temperature enzyme-catalyzed reactions make use of porous organic (like polyvinylchloride) membranes. The use of such membranes is limited to temperatures below 100°C. For high-temperature applications, typical of catalytic processes, metal or inorganic membranes have been utilized.

Some of the earlier applications of catalytic membrane reactor technology involved the use of porous glass membranes. In 1981, Kameyama *et al.* (*3*) utilized porous Vycor Glass tubes to study the decomposition of H_2S to produce H_2 and S. Conversions as high as twice the equilibrium limit were observed. Glass membranes have since then been utilized in other studies for the catalytic dehydrogenation of cyclohexane to benzene over supported Pt catalysts (*4–6*). The problem with glass membranes lies with their mechanical properties, i.e., their brittleness and their poor resistance to thermal and mechanical stresses.

Most of the current literature (primarily

[1] To whom correspondence should be addressed.

0021-9517/92 $3.00

from the Soviet Union and Japan) on catalytic membrane reactor applications involves the use of Pd, Pd alloys with Ru, Ni, and various metals from groups VI to VIII, and Pd-coated zirconia, alumina, and titania membranes. The Soviet literature, in particular, is impressive and includes many Soviet inventor's certificates and European and American patents. They cover a number of hydrogenation and dehydrogenation reactions, such as CH_4 steam reforming (*7*), dehydrogenation of butene to butadiene (*8*), acetylene hydrogenation (*9*), dehydrogenation of 1-, 2-cyclohexanediol (*10*), dehydrogenation of isopropyl alcohol (*11*), hydrogenation of cyclopentadiene to cyclopentene (*12*), *n*-heptane dehydrogenation (*13*), hydrodealkylation of 1,4- and 1,5-dimethylnaphthalene (*14*), and the production of many other specialty chemicals.

The application of Pd membranes is based on the fact that Pd is highly permeable to H_2 (a fact known since Thomas Graham first observed the phenomenon in 1866) but virtually impermeable to other gases and, of course, liquids. The development of Pd membranes has had a significant impact on proving and popularizing the concept of catalytic membrane reactors. The inherently low transmembrane fluxes, however, combined with the high cost of these membranes and phenomena of metal sintering, imbrittlement, and fatigue, have hindered the widespread industrial application of these membranes. Some of the earlier membrane reactor efforts also involved the use of materials, such as nonporous Ag and CaO-stabilized zirconias exhibiting enhanced oxygen anionic conductivity. A variety of reaction processes, primarily partial oxidation reactions, have been tested with some success (*15*).

High-temperature catalytic reactors using porous ceramic membranes are a more recent development. One of the earlier accounts of the use of such a reactor was a paper by Davidson and Salim (*16*) (following a patent by the same group (*17*)), which reported the use of anodic aluminas in catalytic membrane reactor applications for several dehydrogenation reactions. Anodic aluminas are ideally suited for academic investigations of transport and reaction (see Tsotsis *et al.* (*18, 19*)) because they have straight, nonintersecting pores. The existing membranes, however, have unsatisfactory mechanical strength. It is doubtful, therefore, that anodic membranes will ever find significant industrial catalytic membrane reactor applications. A broadly written British patent by Bitter (*20*) claimed the use of Sol-Gel alumina membranes for several dehydrogenation reactions, one of them being the dehydrogenation reaction of propane to propylene, for which they claimed significant improvements in yield. The technical details in the patent are, however, sketchy. No further open literature information has been published, and no U.S. Patent has been issued.

Zaspalis *et al.* (*21–25*) recently reported on the use of Sol-Gel alumina and titania membranes in catalytic membrane reactor applications. Reactions studied included the dehydrogenation of methanol (*21–24*) and *n*-butane (*23*) and the reaction between NO and NH_3 (*21, 25*). Although the use of inorganic membranes did not apper to greatly improve the conversion and yield of the reactions studied, and significant catalyst deactivation was observed, a number of novel concepts were presented, including the use of membrane reactors to prevent catalyst deactivation and maintaining a pressure drop across the membrane to prevent the slip of one of the reactants through the membrane. The latter concept was tested with the NO + NH_3 reaction. The concept of a membrane reactor, which uses a nonpermselective catalytic membrane to provide a well-defined and controlled interface between reactants flowing in opposite sides of the membrane was originally suggested for vapor phase reactions by Sloot *et al.* (*26*) and tested for the Clauss desulphurization process, and by Harold and Cini (*27, 28*) for multiphase reaction systems.

Okubo *et al.* (*29*) recently reported using

an asymmetric hollow fiber alumina membrane for cyclohexane dehydrogenation. The reactor consisted of a bed of $Pt/\gamma\text{-}Al_2O_3$ particles placed on the outside of the membrane filter. The use of a hybrid reactor system consisting of a conventional packed-bed reactor followed by a membrane reactor was also described in that paper. A membrane reactor containing an asymmetric alumina membrane (Membralox) with $Fe_2O_3/\gamma\text{-}Al_2O_3$ catalyst particles, promoted with K_2O, packed in its interior was used by Wu *et al.* (*30*) for dehydrogenation of ethylbenzene to styrene. An improvement in conversion (originally ~15%, more modest gains reported later (*31*)) was reported over the case with no membrane. The use of a similar membrane reactor to attain conversions higher than the corresponding equilibrium conversions for the same reaction was recently reported by Ma *et al.* (*32*).

One of the earliest open literature publications reporting the use of Sol-Gel alumina membranes in a catalytic membrane reactor application is by Champagnie *et al.* (*33*). In this paper, results of preliminary studies of the ethane dehydrogenation reaction in a catalytic membrane reactor were reported. Using a membrane reactor operating in a "cross-flow/counter-flow" configuration and for dilute ethane and hydrogen feed mixtures in Ar, conversions up to six times higher than the corresponding equilibrium conversions, for a region of experimental conditions, were observed. The cross-flow/counter-flow mixed mode membrane reactor is very effective for enhancing reactor yields. It is not convenient to model however. In this paper, a more complete account of our experimental studies of the ethane dehydrogenation reaction in a catalytic membrane reactor is presented. The reactor was operated in a cocurrent-flow mode. A mathematical model is also presented describing the operation of this reactor. The predictions of this model are compared with the experimental findings for both dilute and dense ethane feed mixtures. Ethane dehydrogenation is, of course, a very important industrial reaction used to produce ethylene, a valuable chemical commodity. The predominant industrial process for producing ethylene is homogeneous thermal cracking of ethane at high temperatures, which produces considerable amounts of by-products, such as methane, acetylene, and higher hydrocarbons. The typical selectivity to ethylene, in an ethane steam cracker, is 78 to 82 mol% with recycle. Heterogeneous catalytic processes have also been developed, using platinum supported on alumina catalysts, resulting in higher selectivities to ethylene of up to 98% (*34*). The very high temperatures necessary to obtain adequate yields, however, result in catalyst deactivation, due to metal sintering and coke formation.

EXPERIMENTAL APPARATUS

A schematic of the experimental apparatus is shown in Fig. 1a. It consists of the reactant gas delivery system, the membrane reactor, and the product collection and measurement devices. The ceramic alumina membrane tube (Membralox) is supplied by ALCOA. It consists of a multilayered composite porous alumina tube with an inner diameter of 7 mm, an outer diameter of 10 mm, and a length of 25 cm. The membrane reactor, shown in Fig. 1b, consists of a stainless-steel casing, inside of which the ceramic tube was placed and sealed to the stainless-steel body using graphite string wrapped around the tube. The shellside inlet and outlet openings were situated 17.5 cm apart. They allow for either cocurrent- or countercurrent-flow configurations. A center inlet port makes it possible to also operate the reactor in other flow configurations.

Heating was provided by six 57.5-W semicylindrical heaters, each pair controlled by an Omega CN-2000 programmable temperature controller using a wire thermocouple (Omega) touching the outside ceramic membrane tube surface. Two other thermocouples monitored the temperatures of the inside membrane surface. The reactor was well insulated and was operated under rea-

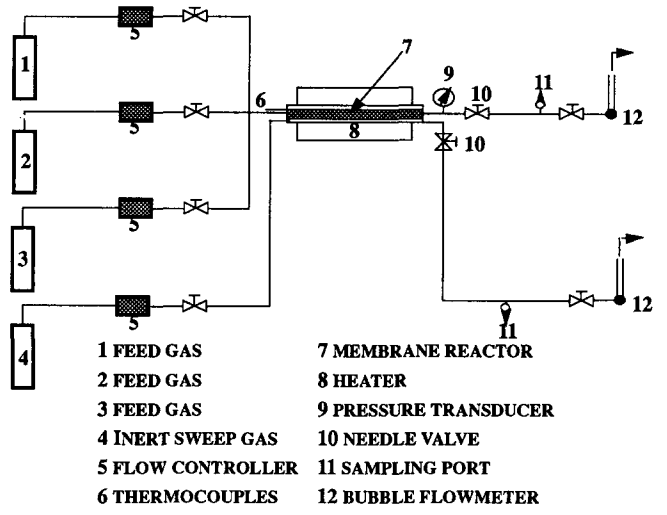

(a)

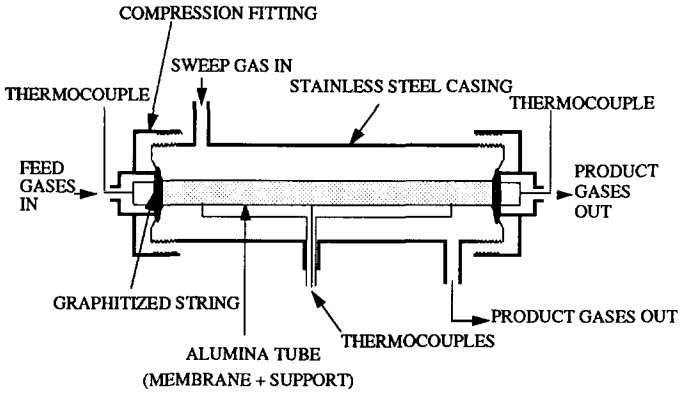

(b)

FIG. 1. (a) Schematic of apparatus, (b) ceramic membrane reactor.

sonably isothermal conditions with all thermocouples readings within 2°C. The reactant gases were dried and purified before being fed through the tubeside inlet. The individual gas flowrates, the mixture composition, and the overall flow rates were controlled by flow controllers. An inert gas, acting as a sweep gas, was allowed into the reactor shellside. The tubeside pressure was controlled by a needle valve on the tubeside outlet and measured by a pressure gauge. The shellside outlet was maintained at atmospheric pressures.

The alumina membrane tube was wet impregnated, using reaction grade 2-hexachloroplatinic acid. For the membranes used in these experiments the impregnation was carried out using a micropipette, drop by drop on the inside surface of the membrane. The Pt metal impregnated on the membrane corresponds to a 5% wt loading based on the weight of the three microporous layers of the composite membrane. Although care was exercised to obtain uniform impregnation both around the periphery and along the length of the mem-

brane, it is possible that local nonuniformities exist in the impregnation profiles. Other impregnation methods (*35, 36*) have also been tried, like placing the impregnating solution in the interior of the membrane or placing the whole membrane inside a beaker containing the impregnation solution. It is not clear whether these alternate impregnation methods result in a more uniform impregnation than the micropipette technique and themselves are associated with a number of additional problems like controlling the amount of metal deposited. The issue of how to properly impregnate a composite catalytic ceramic membrane, in our opinion, remains unresolved.

After impregnation, the membrane was dried overnight and then sealed inside the stainless-steel reactor. A 40 mol% oxygen in argon mixture at 130°C was passed over the catalyst overnight. Subsequently, hydrogen was passed through the reactor at 350°C for 12 h. During experiments to investigate the effect of various reactor parameters, the compositions of the various streams were analyzed on line using a UTI 100C mass spectrometer. Besides ethylene, ethane, and hydrogen, the concentrations of methane and C_3 and larger species were also monitored. The overall flow rates were also measured using glass bubble flowmeters. For the runs under dilute conditions (less than 10% ethane in Ar), there were no detectable amounts of methane or C_3 and higher carbon species observed. For the dense mixtures (over 80% C_2H_6 in Ar) for temperatures of 675°C and higher, the selectivity of ethane to ethylene was 98%. There was, furthermore, a slight decline in catalytic activity. The conversions reported for temperatures of over 675°C were recorded 1 h after the initiation of the steady-state run. The deactivated catalyst could be reactivated by repeated treatments in oxygen and hydrogen.

THEORETICAL MODEL

Figure 2 shows a schematic of the cross section of the reactor. To develop the model for the reactor the following assumptions were made:

1. Isothermal, steady-state conditions prevail everywhere in the reactor.
2. The tubeside and shellside show plug-flow behavior and the flows are cocurrent. The radial tubeside and shellside concentration gradients are negligible.
3. The diffusion resistance of and reaction in the macroporous membrane layer, which exists to support the thin permselective membrane layers, are both negligible.
4. No limitations to mass transfer exist in the gas phase, and the pressure drops in the tubeside and shellside are negligible.
5. Axial diffusion in the membrane is negligible compared to the radial diffusion term.

Assumption (1) was reasonably well satisfied for all experimental runs reported here, as was assumption (3). *In situ* permeability studies with the impregnated membranes showed that over 90% of the resistance to diffusion resulted from the microporous permselective layers (*37*). The ratio, furthermore, of the surface area of the support to that of the three permselective layers is less than 0.01. Assumption (5) is based on the fact that the thickness to length ratio of the permselective membrane layers is of the order of 10^{-3} and the ends of the membrane are impermeable to flow. It is difficult to completely verify through independent experiments assumptions (2) and (4), the validity of which is obviously dependent on the shellside and tubeside residence times. For the residence times reported here diffusion in the axial direction was negligible compared to convective flow and there were no measureable pressure drops. In addition, the temperatures inside the reactor measured along the center axis and near the membrane surface on both sides of the center line indicate that the temperature profile is flat. On the other hand, little evidence exists that the velocity profile is flat. The length to diameter ratio of 33 would tend to indicate that for the most part inside the reactor the flows would not be well devel-

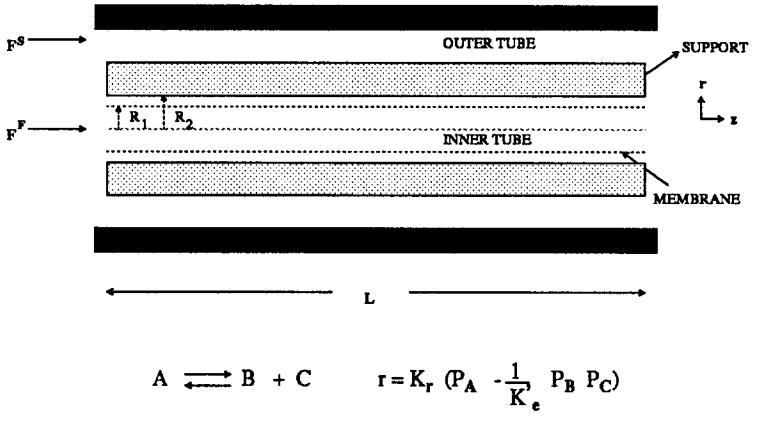

FIG. 2. Schematic of reactor cross section.

oped. Reynolds number calculations indicate that laminar flow conditions should prevail, but the presence of permeable walls should tend to flatten the velocity profiles.

Inside the Membrane

$$\frac{D_j}{\mathrm{RT}}\frac{1}{r}\frac{d}{dr}\left[r\frac{dP_j}{dr}\right] = -\nu_j k_r\left[P_A - \frac{P_B P_C}{K'_e}\right], \tag{1}$$

where D_j is the effective Knudsen diffusivity of component j; k_r is the reaction constant; K'_e is the equilibrium constant; P_j is the partial pressure of species j, with A standing for ethane, B for ethylene, C for hydrogen, and I for inerts; r is the radial coordinate; and ν_j is the stoichiometric coefficient, where $\nu_j < 0$ for reactants, $\nu_j > 0$ for products, and $\nu_j = 0$ for inerts. The boundary conditions for Eq. (1) are

$$P_j = y_j^{\mathrm{F}} P_t^{\mathrm{F}} \quad \text{at } r = R_1 \tag{1a}$$

$$P_j = y_j^{\mathrm{S}} P_t^{\mathrm{S}} \quad \text{at } r = R_2, \tag{1b}$$

where y_j^{F}, y_j^{S} are the mole fractions for species j in the feedside (tubeside) and shellside correspondingly. P_t^{F}, P_t^{S} are the corresponding total pressures. In the model, P_t^{F}, P_t^{S} are assumed to be constant along the length of the reactor. Generally, however, $P_t^{\mathrm{F}} \neq P_t^{\mathrm{S}}$. R_1 and R_2 are the inner and outer diameters of the reactive membrane layer.

The rate expression on the right side of Eq. (1) and the kinetic constant k_r were derived by independent *in situ* investigations of the reaction kinetics of the ethane to ethylene reaction. In these experiments the reactor was operated with the shellside inlet and outlet closed. The membrane temperature and tubeside residence time and concentration were varied and the reactor conversion was measured. The data were fitted to a rate expression of the form shown in Eq. (1). k_r was found to obey

$$k_r = A \exp\left[-\frac{E}{\mathrm{RT}}\right], \tag{2}$$

where $A = 4.56 \times 10^4$ gmol/(cm^3 · atm · s) and the activation energy $E = 20.61$ kcal/gmol (see (*37*) for further details).

The thermodynamic equilibrium constant, K'_e, calculated by traditional techniques, was found to obey the relationship

$$K'_e = A_e \exp\left[-\frac{E_e}{\mathrm{RT}}\right], \tag{3}$$

where $A_e = 1.096 \times 10^7$ atm and $E_e = 34.26$ kcal/gmol.

In the Tubeside

$$\frac{dn_j^{\mathrm{F}}}{dz} = 2\pi\frac{D_j}{\mathrm{RT}}\left[r\left(\frac{dP_j}{dr}\right)\right]_{r=R_1}. \tag{4}$$

The initial condition at $z = 0$ is

$$n_j^F = n_{j0}^F = F_0^F(y_{j0}^F P_t^F/RT), \qquad (4a)$$

where n_j^F is the molar flow rate of species j at z, n_{j0}^F is its inlet molar flow rate, F_0^F is the inlet total volumetric flow rate and y_{j0}^F its inlet mole fraction in the feedside. The rest of the symbols have been previously defined; their definitions can also be found in the Appendix.

In the Shellside

$$\frac{dn_j^S}{dz} = -2\pi \frac{D_j}{RT}\left[r\left(\frac{dP_j}{dr}\right)\right]_{r=R_2} \qquad (5)$$

$$\text{with } n_j^S = n_{j0}^S = F_0^S \frac{y_{j0}^S P_t^S}{RT} \text{ at } z = 0. \qquad (5a)$$

The symbols have the same meaning as above, with superscript S signifying the shellside.

The following dimensionless variables are defined:

$$P_r = \frac{P_t^S}{P_t^F}, \quad X_j = \frac{P_j}{P_t^F}, \quad \psi_j^F = \frac{n_j^F}{n_0^F}, \quad \psi_j^S = \frac{n_j^S}{n_0^F},$$

$$\xi = \frac{r}{R_1}, \quad \omega = \frac{\ln \xi}{\alpha}$$

$$\left(\text{with } \alpha = \ln(1+\varepsilon), \text{ where } \varepsilon = \frac{R_2 - R_1}{R_1}\right)$$

$$\Phi = \alpha R_1 \sqrt{\frac{k_r RT}{D_A}},$$

$$\delta_j = \frac{D_j}{D_A}, \quad K_e = \frac{K_e'}{P_t^F}, \quad \zeta = \frac{z}{L},$$

$$Q = \frac{2\pi D_A L}{F_0^F}, \quad F_r = \frac{F_0^S}{F_0^F}.$$

The ratio of the shellside and feedside total pressures, P_r, and the ratio of the shellside and feedside inlet flow rates, F_r, are set experimentally. The characteristic membrane parameter, ε, is equal to the ratio of the thickness of the permselective layer to the radius of the membrane tube; Φ is the Thiele modulus for the membrane; and Q is a dimensionless group, equal to the ratio of the maximum possible diffusional flux of the species A through the membrane (in the absence of reaction and for conditions prevailing throughout the membrane being the same with those at the inlet) to the total inlet molar flow rate.

Based on the above definitions Eqs. (1)–(5) become:

In the Membrane

$$\frac{d^2X_j}{d\omega^2} = -(\nu_j/\delta_j)\exp(2\alpha\omega)\Phi^2 \left(X_A - \frac{1}{K_e}X_B X_C\right) \qquad (6)$$

$$X_j = y_j^F \quad \text{at } \omega = 0 \qquad (6a)$$

$$X_j = y_j^S P_r \quad \text{at } \omega = 1. \qquad (6b)$$

In the Tubeside

$$\frac{d\psi_j^F}{d\zeta} = \frac{Q\delta_j}{\alpha}\left(\frac{dX_j}{d\omega}\right)_{\omega=0} \qquad (7)$$

$$\psi_j^F = y_{j0}^F \quad \text{at } \zeta = 0. \qquad (7a)$$

In the Shellside

$$\frac{d\psi_j^S}{d\zeta} = -\frac{Q\delta_j}{\alpha}\left(\frac{dX_j}{d\omega}\right)_{\omega=1} \qquad (8)$$

$$\psi_j^S = F_r P_r y_{j0}^S \quad \text{at } \zeta = 0. \qquad (8a)$$

From Eq. (6), adding together the equations for A and B and A and C and integrating, one obtains the following system of two algebraic equations, which relate X_B and X_C to X_A.

$$\delta_B X_B = (P_r y_A^S - y_A^F + \delta_B(P_r y_B^S - y_B^F))\omega + y_A^F + \delta_B y_B^F - X_A \qquad (9)$$

$$\delta_C X_C = (P_r y_A^S - y_A^F + \delta_C(P_r y_C^S - y_C^F))\omega + y_A^F + \delta_C y_C^F - X_A \qquad (10)$$

The three differential equations (6) corresponding to species A, B, C can be replaced by the algebraic equations (9) and (10) and the following differential equation.

$$\frac{d^2X_A}{d\omega^2} = \Phi^2\exp(2\alpha\omega)\left[X_A - \frac{1}{K_e\delta_B\delta_C}\right.$$
$$\left.[(y_A^S P_r + \delta_B y_B^S P_r - y_A^F - \delta_B y_B^F)\omega\right.$$

$$+ (y_A^F + \delta_B y_B^F) - X_A][(y_A^S P_r + \delta_C y_C^S P_r - y_A^F - \delta_C y_C^F)\omega + (y_A^F + \delta_C y_C^F) - X_A]\Big] \quad (11)$$

$$X_A = y_A^F \quad \text{at } \omega = 0 \quad (11a)$$

$$X_A = y_A^S P_r \quad \text{at } \omega = 1. \quad (11b)$$

The corresponding equation for the inert component is

$$\frac{d^2 X_I}{d\omega^2} = 0 \quad (12)$$

$$X_I = y_I^F \quad \text{at } \omega = 0 \quad (12a)$$

$$X_I = y_I^S \quad \text{at } \omega = 1, \quad (12b)$$

where by simple integration

$$X_I = (y_I^S P_r - y_I^F)\omega + y_I^F. \quad (13)$$

The system of Eqs. (7)–(12) was solved using a numerical technique that combined a finite difference method with variable step size and deferred conditions to solve Eqs. (9)–(12) (IMSL version 10.0 subroutine DBVFD) and a third-order Runge Kutta technique to solve Eqs. (7) and (8). Note, however, that for thin membranes $\exp(2\alpha\omega) \sim 1$ and for small and large values of Φ regular and singular perturbation analytical solutions can be developed to solve Eqs. (9)–(12). Only for a narrow region of Φ values does one really need to solve the full system of Eqs. (9)–(12) numerically. The exact numerical details can be found elsewhere (*37*).

EXPERIMENTAL RESULTS AND DISCUSSION

All the experiments reported here were performed with one single membrane. This was an asymmetric composite Sol-Gel type membrane provided to us by ALCOA (Membralox). The membrane consisted of four layers, the nominal diameters and thicknesses of which are reported in Fig. 3.

Two gas feed compositions were used during the membrane reactor experiments. The first feed composition called the dilute feed, consisted of 8.7 mol% ethane, 4.4 mol% hydrogen, and 86.9 mol% argon. The second feed composition, defined as the dense feed, consisted of 83.4 mol% ethane, 8.3 mol% hydrogen, and 8.3 mol% argon. Further details of the gas composition analysis techniques can be found elsewhere (*37*).

The membrane was impregnated with Pt as previously described in the experimental section. The total amount of Pt on the membrane was 32 mg. Based on the surface area ratios one would expect over 80% of this metal to be deposited in the first two layers of the membrane. The impregnation method, as described earlier, would also favor the deposition in the first two layers. This was verified by direct visual inspection and by SEM analysis of cross sections of the membrane. Since these experiments were completed, a detailed study of the effect of the various impregnation parameters on the metal distribution in these membranes and the relationship between metal distribution profiles and membrane activity and permeability has been initiated. Results of this study will be reported in a future publication.

Before the initiation of the membrane reactor experiments, detailed kinetic investigations were performed in order to derive the reaction rate expression and to calculate the values of the kinetic constants. The kinetic experiments were performed in the membrane reactor with the shellside inlet and outlet closed. The ethane conversion to ethylene was measured for different feed concentrations and temperatures and tubeside residence times. The model used for data analysis is described in (*37*). The reaction rate expression found to give the best fit to the data and the values of the rate and equilibrium constants have already been given in the Theoretical Model section.

The permeability of all species involved in the reaction was also measured in the temperature range 25–400°C. Experimental details of the permeability measurement technique have already been reported (*33*). For temperatures above 250°C for the impregnated membranes and pressure gradients across the membrane of up to 1 atm,

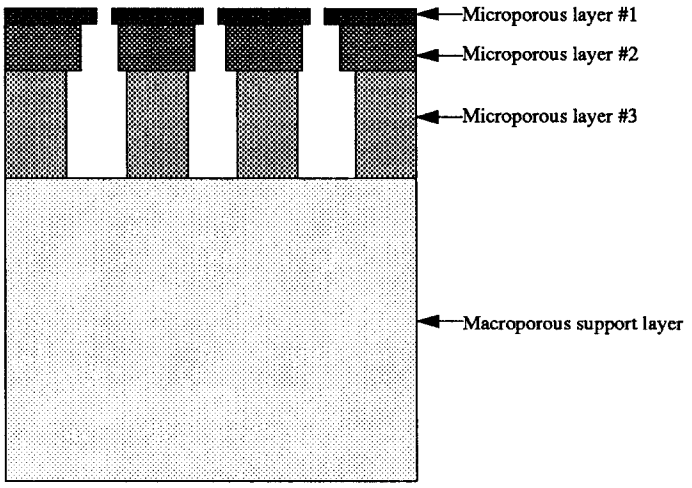

LAYER	Pore Diameter	Layer Thickness	Porosity
1	40 A	5 microns	0.53
2	2000 A	30 microns	0.53
3	8000 A	50 microns	0.53
Support	15 microns	1.5 mm	0.45

FIG. 3. Membralox tube cross section.

all four gases (ethane, hydrogen, ethylene, argon) follow a Knudson type diffusion with diffusivities being inversely proportional to the square root of their molecular weights. For temperatures higher than 400°C the permeabilities for ethane and ethylene were extrapolated using the Knudsen formula (*38*), i.e.,

$$D_k = k_0 \left(\frac{T}{M}\right)^{1/2}. \qquad (14)$$

The first series of membrane reactor experiments involved the study of the effect of sweep ratio F_r on ethane conversion. The dilute feed was used together with a reactor temperature of 550°, a residence time of 2.15 s, and a tubeside pressure of 2 atm. The shellside pressure was kept at 1 atm. Pressure drops along the length of either the shellside or the tubeside were negligible (less than 0.03 atm). The data, for sweep ratios ranging from 0.5 to 2.0, are shown in Fig. 4.

Shown also on this figure are the values of the homogeneous thermodynamic equilibrium conversions (X_{eq}) at the tubeside and shellside pressure conditions. The solid line represents the model fit. The only adjustable parameter used to fit these data was the thickness of the permselective layer. The thickness value used to draw the solid line is 13 μm. This is 2.6 times higher than the nominal thickness of the first microporous layer. The preparation methods, however, of the Sol-Gel membranes, result in an interfacial region between layers, in which the top layer penetrates into the bottom layer. Given the uncertainty in the measurement of the layers' thickness and the fact that

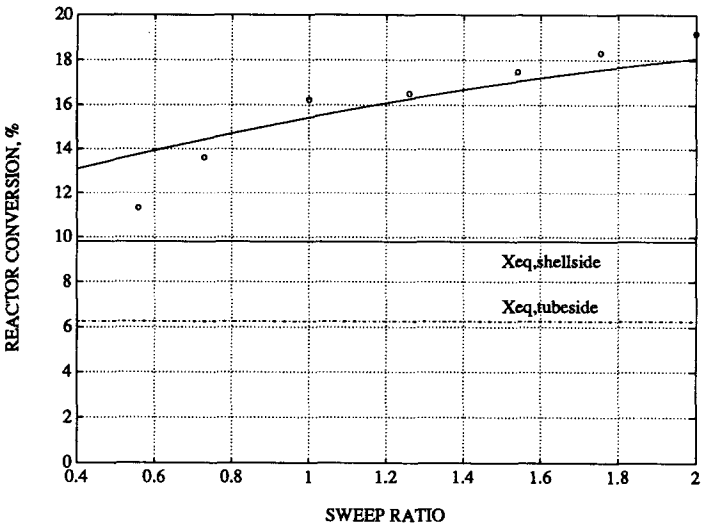

FIG. 4. Conversion vs sweep ratio for the dilute feed; $T = 550°C$, $\tau = 2.15$ s, $P_t^F = 2$ atm, $P_t^S = 1$ atm.

some contribution of the second layer, both in terms of activity and resistance to flow, is to be expected, the estimated value of the thickness of the permselective layer is reasonable. The same value for the thickness was used in all subsequent figures in this paper; i.e., no further adjustment was made to improve the fit.

The behavior shown in Fig. 4 was expected. Increasing the flow rate of the inert gas in the shellside, while keeping the tubeside residence time constant, decreases the concentration of hydrogen in the shellside and, therefore, increases the rate of the hydrogen depletion rate from the vicinity of the catalyst. Lower hydrogen pressures in the catalyst's vicinity result in higher reaction rates. This is clearly shown in Figs. 5a and 5b, where the calculated hydrogen and ethane partial pressures along the length of the membrane in the shellside and tubeside are shown as a function of the sweep ratio (the dotted line is for sweep ratio of 1 and the solid line for sweep ratio of 2). Here, the hydrogen partial pressure initially drops at a faster rate in the tubeside at higher sweep ratios as a result of the lower shellside partial pressures of hydrogen and the corresponding increased flux of hydrogen from the tube to the shellside. The driving force for diffusion is highest at the entrance of the reactor, where the shellside hydrogen partial pressure is close to zero. The rate of diffusion of hydrogen across the membrane is highest in the first 25% of the reactor length, after which it begins to level off. At a distance of 0.75 reactor lengths, the rate of diffusion of hydrogen across the membrane has slowed down to 20% of the initial rate.

Figure 6 shows the calculated overall reactor conversion at various distances z from the inlet of the reactor. The overall conversion at point z is defined as the total amount of ethane consumed up to that point along the reactor length. The results show that up to 80% of the overall conversion occurs in the first half of the reactor. This is due to the high reaction rate resulting from the enhanced diffusion of hydrogen across the membrane in the first half of the reactor.

Figure 7 shows the effect of membrane temperature on reactor conversion as measured experimentally in the reactor. The solid line again represents the model calculations for a permselective layer thickness of 13 μm. The rest of the membrane reactor parameters are indicated in the figure cap-

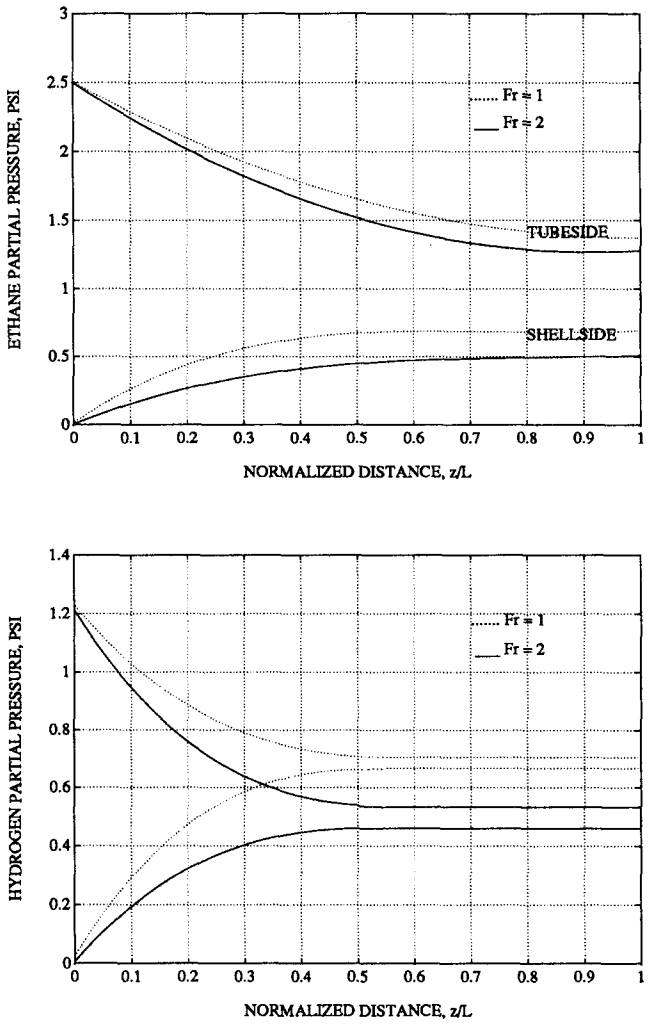

FIG. 5. Partial pressure vs distance along reactor for dilute feed; . . . F_r = 1.0, —F_r = 2.0. Other conditions same as in Fig. 4.

tion. As expected the membrane reactor conversion increases as a function of membrane temperature due to the resulting higher reaction rates.

The effect of tubeside pressure on reactor conversion, while keeping the shellside pressure and all other conditions constant (as indicated in the figure caption), is shown in Fig. 8. Increasing the tubeside pressure generally decreases the reactor conversion, a trend also seen with X_{eq}.

Figure 9 shows the effect of tubeside residence time on reactor conversion. Increasing the tubeside residence time increases the reactor conversion. This behavior is due to the increased contact time between the reactants and the catalyst in the membrane.

If by increasing the residence time the reactor conversion is increased, then a longer reactor length should also produce a similar conversion increase. The model can be used to study the effect of increasing the reactor length on the overall conversion. An

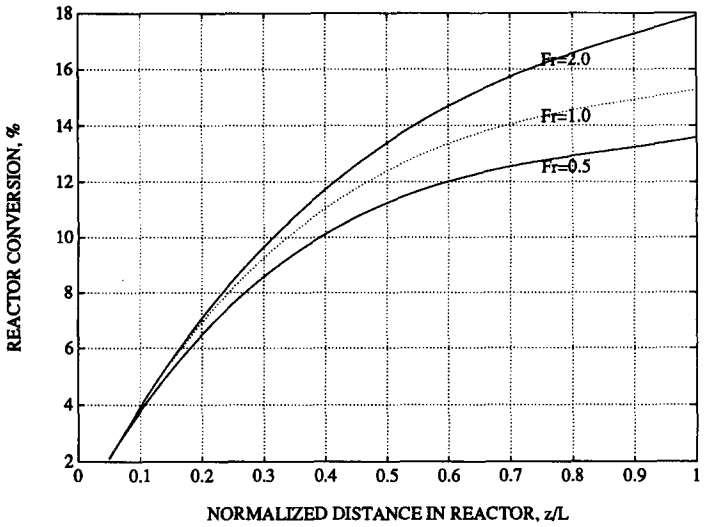

FIG. 6. Conversion vs distance along the reactor length; T = 550°C, τ = 2.15 s, P_t^F = 2 atm, P_t^S = 1 atm.

increase in the reactor length produces an increase in the overall conversion as can be seen in Fig. 10a. (In this figure, the tubeside residence time was kept constant at 2.15 s for all reactor lengths by adjusting the flow rate.) There is obviously a reactor length beyond which increasing the reactor length produces no marked improvement in conversion due to the eventual back diffusion of product gases, which offsets the increase in ethane reaction due to the increasing amount of catalyst. For example in Fig. 10b for a temperature of 550°C, sweep ratio of 1.0, tubeside pressure of 2 atm, and dilute feed conditions, increasing the reactor length of 12.5 cm by a factor of 2.0 almost

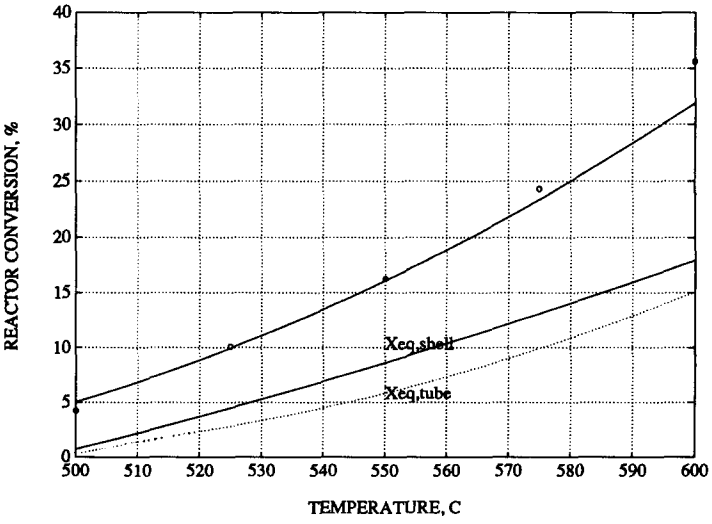

FIG. 7. Conversion vs temperature for the dilute feed; F_r = 1.0, τ = 2.15 s, P_t^F = 2 atm, P_t^S = 1 atm.

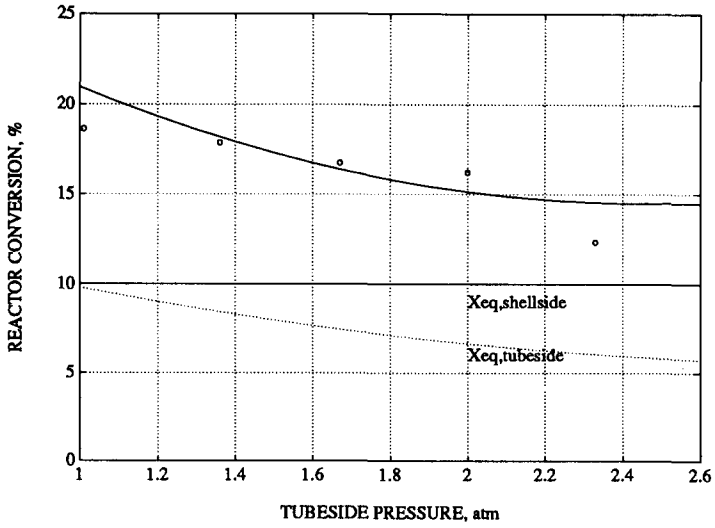

FIG. 8. Conversion vs tubeside pressure for the dilute feed; T = 550°C, F_r = 1.0, τ = 2.15 s, P_t^S = 1 atm.

doubles the overall conversion. However, doubling the reactor length further from 25.0 to 50.0 cm produces only an additional 20% increase over the conversion obtained in the reactor with a length of 25.0 cm.

The thickness of the permselective membrane layer is a variable, which also affects the maximum conversion obtainable in the reactor. The thickness affects the flux of gases through the membrane and affects the reaction rates. As the thickness increases, the reactor conversion increases due to the higher reaction rate resulting from the larger amount of catalyst in the membrane layer. This, however, is counterbalanced by the

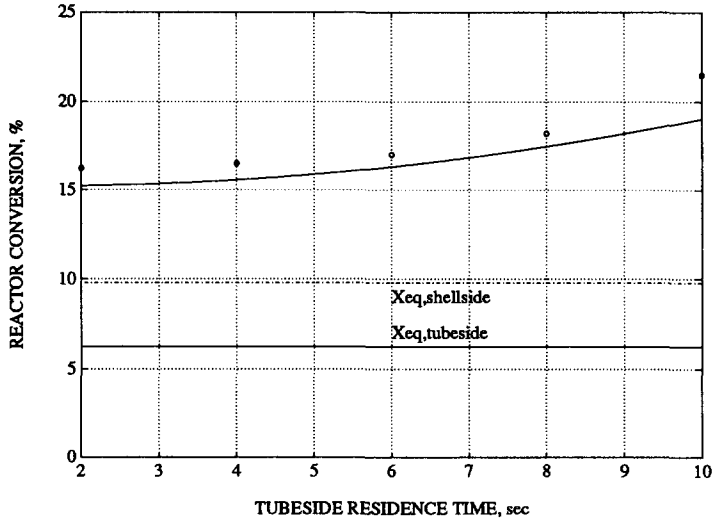

FIG. 9. Conversion vs tubeside residence time for the dilute feed; T = 550°C, F_r = 1.0, P_t^F = 2 atm, P_t^S = 1 atm.

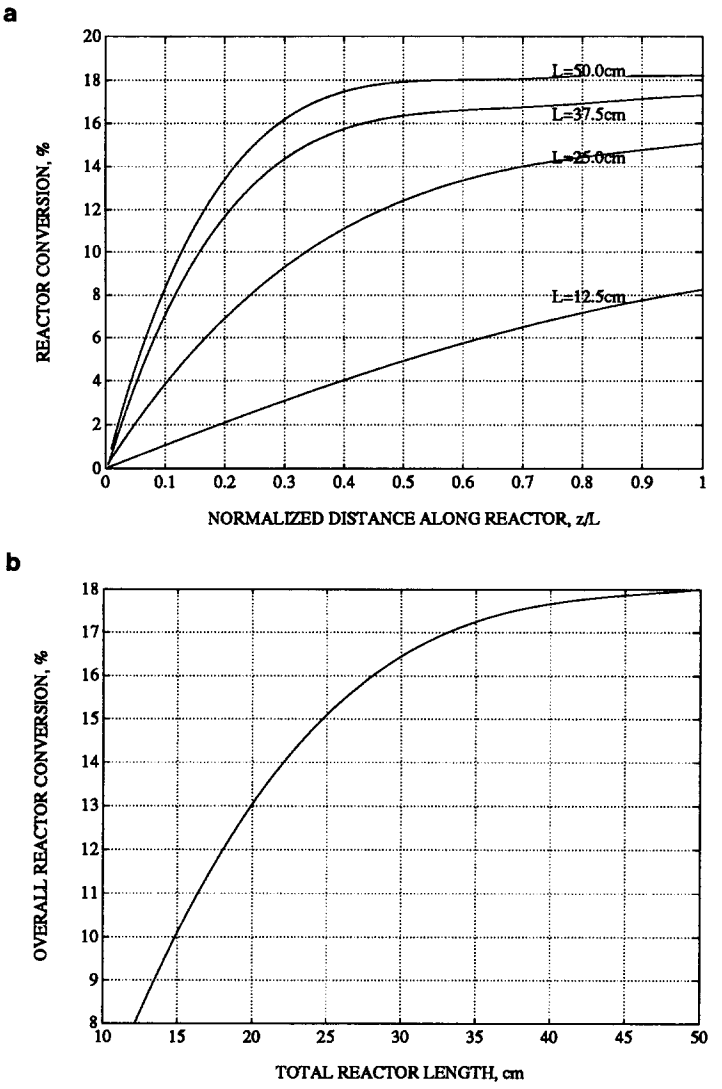

FIG. 10. (a) Calculated conversion vs distance along the reactor length for the dilute feed for various reactor lengths; T = 550°C, F_r = 1.0, τ = 2.15 s, P_t^F = 2 atm, P_t^S = 1 atm. (b) Calculated overall conversion vs total reactor length for the dilute feed; T = 550°C, F_r = 1.0, τ = 2.15 s, P_t^F = 2 atm, P_t^S = 1 atm.

reduced flux of hydrogen through the permselective layer, which results in lower conversions. Optimizing the thickness, residence time, and reactor length for a given set of reaction conditions is obviously important in achieving the maximum yield possible.

Finally, Figs. 11 to 13 present the runs under the dense conditions. Figure 11, in particular, shows the effect of temperature on conversion; Fig. 12 shows the effect of sweep ratio; and Fig. 13 shows the effect of tubeside pressure. This behavior is generally the same as the behavior shown with the dilute feed. The model fit is, however, not as good.

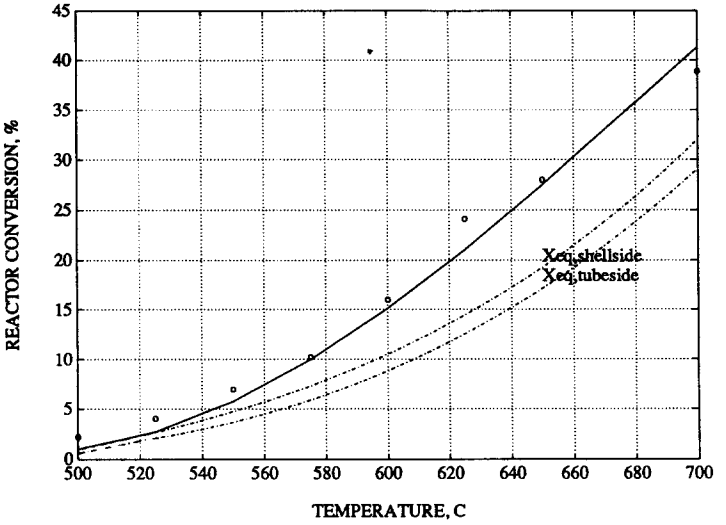

FIG. 11. Conversion vs temperature for the dense feed; $F_r = 1.0$, $\tau = 2.15$ s, $P_t^F = 2$ atm, $P_t^S = 1$ atm.

CONCLUSIONS

Results of studies of the catalytic ethane dehydrogenation in a membrane reactor are presented here. A mathematical model is also presented, which appears to fit the data reasonably well over a broad range of experimental conditions using only one adjustable parameter, i.e., the thickness of the permselective membrane layer. Calculated hydrogen and ethane partial pressures and overall rates along the length of the reactor are also presented as a function of the various reactor parameters. They are helpful in explaining the membrane reactor behavior.

The membrane reactor configuration de-

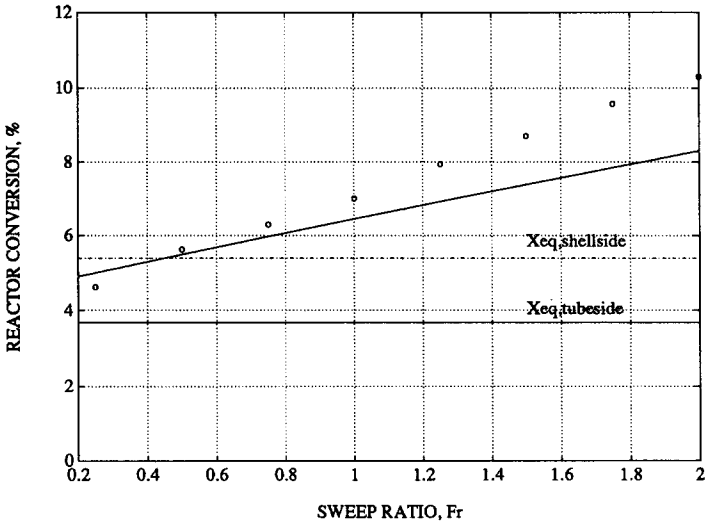

FIG. 12. Conversion vs sweep ratio for the dense feed; $T = 550$°C, $\tau = 2.15$ s, $P_t^F = 2$ atm, $P_t^S = 1$ atm.

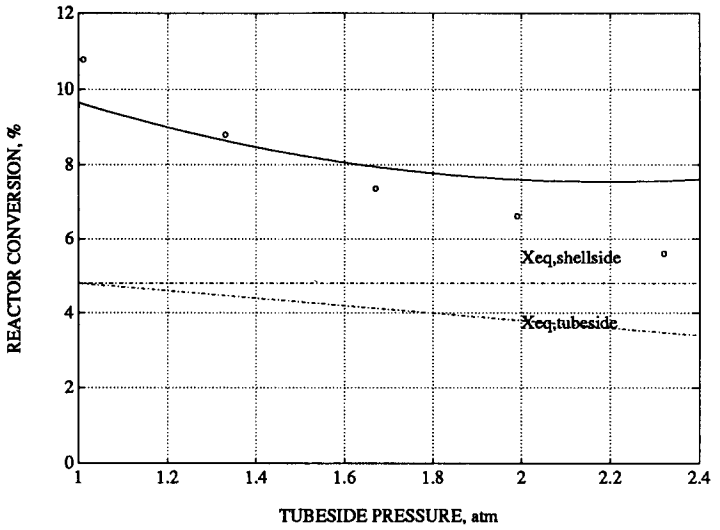

FIG. 13. Conversion vs pressure for the dense feed; T = 550°C, F_r = 1.0, τ = 2.15 s, P_t^S = 1 atm.

scribed here (empty impregnated tube, cocurrent flow) is only one of many possible arrangements. Other membrane reactor configurations involve countercurrent and mixed mode cocurrent/countercurrent configurations. For some reactions, using reactors containing unimpregnated membranes packed with catalyst is more efficient. For others one would opt for packed and impregnated membrane reactors. In industrial practice one would use multitube configurations. In future publications the various design issues associated with the operation of these different catalytic membrane reactor configurations will be addressed.

ACKNOWLEDGMENTS

The financial support of Medalert, Inc., is gratefully acknowledged. We also thank ALCOA Separation Technology Division for providing us with the ceramic membranes and Drs. I. A. Webster of UNOCAL and P. K. T. Liu of ALCOA for many helpful discussions.

APPENDIX: NOMENCLATURE

C_j concentration of species j, mol/cm^3
D_j effective diffusivity for component j, cm^2/s
F^F feed or tubeside volume flow rate, cm^3/s
F_0^F tubeside volume flow rate at inlet, cm^3/s
F^S inert sweep gas volume flow rate, cm^3/s
F_0^S inert sweep gas volume flow rate at inlet, cm^3/s
F_r sweep ratio (F_0^S/F_0^F), dimensionless
K_e' equilibrium constant, atm
K_e equilibrium constant, dimensionless $= K_e'/P_F$
k_r reaction rate constant, gmol/cm^3 · atm^2 · s
L length of membrane, cm
M_j molecular weight of component j
n_j molar flow rate of component j, gmol/s
n_0^F total inlet molar flow rate in tubeside, gmol/s
P_j partial pressure of component j, atm
P_r P_t^S/P_t^F, dimensionless
P_t^F total pressure in the feed or tubeside, atm
P_t^S total pressure in the permeate or shellside, atm
Q $2\pi D_A L/F_0^F$, dimensionless
r radial distance, cm
R universal gas constant, 82.05 cm^3 · atm/gmol · K

R_1 inner radius of membrane element, cm
R_2 outer radius of membrane element, cm
t thickness of membrane layer, cm
T operating temperature, K
V_r volume of inner tube ($\pi R_1^2 L$), cm^3
W weight of catalyst, g
X_{eq} equilibrium conversion, dimensionless
X_j mole fraction of component j in membrane (P_j/P_t^F)
y_j^F mole fraction of component j in the tubeside (n_j^F/n^F)
y_j^S mole fraction of component j in the shellside (n_j^S/n^S)
z longitudinal distance, cm

Greek Symbols

α $\ln(1 + \varepsilon)$, dimensionless
δ_j diffusivity ratio (D_j/D_A), dimensionless
ε $(R_2 - R_1)/R_1$, dimensionless
ζ dimensionless length (z/L)
ν_j stoichiometric coefficient of component j, dimensionless
ξ dimensionless radius (r/R_1)
τ residence time (V_r/F_0^F), s.
ρ gas density, g/cm^3
ψ_j^F n_j^F/n_0^F, dimensionless
ψ_j^S n_j^S/n_0^F, dimensionless
Φ Thiele modulus ($R_1\sqrt{k_r RT/D_A}$), dimensionless
ω $\ln \zeta/\alpha$, dimensionless

Superscript

F refers to the feed or tubeside
S refers to the permeate or shellside

Subscript

A C_2H_6
B C_2H_4
C H_2
I Ar
j component letter
0 refers to inlet conditions

REFERENCES

1. Williams, T. E., Catapano, G., Klein, E., and Ward, R. A., *AIChE Symp. Ser.* **268**(85), 1 (1989).
2. Shao, S., Hu, S., and Govind, R., *AIChE Symp. Ser.* **268**(85), 85 (1989).
3. Kameyama, T., Dokiya, M., Fujishige, M., Yokokama, H., and Fukuda, K., *Ind. Eng. Chem. Fundam.* **20,** 97 (1981).
4. Itoh, N., Shindo, Y., Haraya, K., and Hakuta, T., *Sekiyu Gakkaishi* **32**(1), 47 (1989).
5. Itoh, N., Shindo, Y., Haraya, K., and Hakuta, T., *J. Chem. Eng. Jpn.* **21**(4), 399 (1988).
6. Nagamoto, H., and Inoue, H., *Chem. Eng. Commun.* **34,** 315 (1985).
7. Nazarkina, E. B., and Kirichenko, N. A., *Khim. Teknol. Topl. Masel.*, **3,** 5 (1979).
8. Gryaznov, V. M., Pavlova, L. F., Juarez, E., and Rivera, P., *Dokl. Akad. Nauk. SSSR* **194**(2), 355 (1970).
9. Gul'yanova, S. G., Gryaznov, V. M., Morales, A.Kh., and Fillippov, A. M., Tr. 4-go Sov.-Frants. Seminara po Katalizu, 1. Katalitich. Aktivnost Chist. i Nanesen. Met. 2. Katalitich. Aktivnost Ionov Perekhodn. Met. v Kompleksakh i Okisn. Matritsakh Tbilisi, pp. 126–130, 1978; from *Ref. Zh. Khim.*, Abstr. No. 15B1273 (1979).
10. Mischenko, A. P., Smirnov, V. S., and Gryaznov, V. M., *Isv. Akad. Nauk. SSSR, Ser. Khim.* **7,** 1620 (1970).
11. Mikhalenko, N. N., Khrapova, E. V., and Gryaznov, V. M., *Neftekhimiya* **18**(3), 354 (1978).
12. Zhernosek, V. M., Mikhalenko, N. N., Seyum, I., Khrapova, E. V., and Gryaznov, V. M., *Kinet. Katal.* **20**(4), 921 (1979).
13. Gryaznov, V. M., *Platinum Metals Rev.* **30**(2), 68 (1986).
14. Lebedeva, V. I., *Met. Splavy Kak Membran. Katalizatory M.*, 112 (1981); from *Ref. Zh. Khim.*, Abstr. No. 21B1284 (1982).
15. Hazburn, E. A., *US Patent* 4,791,079 (1988).
16. Davidson, A. P., and Salim, M., *British Ceram. Proc.* **43,** 119 (1988).
17. Furneaux, R. C., Davidson, A. P., and Ball, M. D., Eur. Pat. 244,970 (1987).
18. Tsotsis, T. T., Nourbarkhsh, N., Champagnie, A. M., and Webster, I. A., *AIChE Symp. Ser.* **268**(85), 78 (1989).
19. Tsotsis, T. T., Nourbarkhsh, N., and Webster, I. A., *Prepr. Pap.-Am. Chem. Soc., Div. Petrol. Chem.* **33**(3), 502 (1989).
20. Bitter, J. G. A., Brit. Patent GB 2,201,159 (1988).
21. Zaspalis, V. T., Ph.D. thesis, University of Twente, The Netherlands, 1990.
22. Zaspalis, V. T., van Praag, W., Keizer, K., van Ommen, J. G., Ross, J. R. H., and Burggraaf, A. J., *Appl. Catal.* **74,** 205 (1991).
23. Zaspalis, V. T., van Pragg, W., Keizer, K., van Ommen, J. G., Ross, J. R. H., and Burggraaf, A. J., *Appl. Catal.* **74,** 223 (1991).
24. Zaspalis, V. T., van Praag, W., Keizer, K., van

Ommen, J. G., Ross, J. R. H., and Burggraaf, A. J., *Appl. Catal.* **74,** 235 (1991).
25. Zaspalis, V. T., van Praag, W., Keizer, K., van Ommen, J. G., Ross, J. H., and Burggraaf, A. J., *Appl. Catal.* **74,** 249 (1991).
26. Sloot, H. J., Versteeg, G. F., and van Swaaij, W. P. H., *Chem. Eng. Sci.* **45,** 2415 (1990).
27. Harold, M. P., and Cini, P., *AIChE Symp. Ser.* **85,** 26 (1989).
28. Harold, M. P., and Cini, P., *AIChE J.* **37,** 997 (1991).
29. Okubo, T., Haruta, K., Kusakabe, K., Morooka, S., Anzai, H., and Akiyama, S., *Ind. Eng. Chem. Res.* **30**(4), 614 (1991).
30. Wu, J. C. S., Gerdes, T. E., Pszczolkowski, J. L., Bhave, R. R., and Liu, P. K. T., *Sepn. Sci. Technol.* **25,** 1489 (1990).
31. Gallaher, G. R., Gerdes, T. E., and Liu, P. K. T., *Sepn. Sci. Technol.,* in press.
32. Ma, Y. H., Becker, Y. L., Moser, W. R., and A. G., *in* "Proceedings, 2nd International Conference on Inorganic Membranes, Montpellier, France, 1991," in press.
33. Champagnie, A. M., Tsotsis, T. T., Minet, R. G., and Webster, I. A., *Chem. Eng. Sci.* **45**(8), 2423 (1990).
34. Vora, B. V., Pujado, P. R., and Anderson, R. F., *Energy Prog.* **6**(3), 171 (1986).
35. Santacesaria, E., Carra, S., and Adami, I., *Ind. Eng. Chem., Prod. Res. Dev.* **16**(1), 41 (1977).
36. Sceiza, O. A., Castro, A. A., Ardiles, D. A., and Parerna, J. M., *Ind. Eng. Chem. Fundam.* **25,** 84 (1986).
37. Champagnie, A. M., Ph.D. thesis, University of Southern California, 1991.
38. Satterfield, C. N., "Mass Transfer In Heterogeneous Catalysis." MIT Press, Cambridge, MA, 1970.